International Journal of Information, Control and Computer Sciences
ISSN: 2517-9942
Vol:6, No:12, 2012

Autonomous Control of Multiple Mobile Manipulators

Shonal Singh, Bibhya Sharma, Jito Vanualailai, and Avinesh Prasad

***Abstract*—**This paper considers the autonomous navigation problem of multiple *n*-link nonholonomic mobile manipulators within an obstacle-ridden environment. We present a set of nonlinear acceleration controllers, derived from the Lyapunov-based control scheme, which generates collision-free trajectories of the mobile manipulators from initial configurations to final configurations in a constrained environment cluttered with stationary solid objects of different shapes and sizes. We demonstrate the efficiency of the control scheme and the resulting acceleration controllers of the mobile manipulators with results through computer simulations of an interesting scenario.

***Keywords*—**Artificial potential fields, kinodynamic constraints, Lyapunov-based control scheme, Lyapunov stability, minimum distance technique, nonholonomic manipulator.

I. Introduction

THE autonomous navigation of multi-agents, or multiple robots, in obstacle-ridden, or real-world, environments has been an active research domain for at least two decades now due to its wide-ranging capabilities and abundance of real-world applications [1]. A few prominent applications of multi-agent research include surveillance, reconnaissance, construction, warehouse moving, transportation, healthcare, mining, and planetary exploration. These applications invariably demand a high rate of system effectiveness [2], thus, this requirement is one of the main motivations of employing multi-agents. That is, with respect to a single agent, multi-agents can perform an allocated task more efficiently in terms of time and quality, easily accomplish tasks not executable by a single robot and has the benefits of highly distributed sensing and actuation. Also, instead of utilizing a single powerful robot (or *superbot*) to perform a complex task, multi-agents can be easier and cheaper, and can also provide flexibility to task execution and robustness [2].

Devising motion planning algorithms for multi-agents sharing acommon workspace is inherently difficult because the environmentis no longer static but dynamic. The dynamic environment includesboth the stationary and the unpredictable (or predictable) dynamicobstacles [1]. These dynamic obstacles can includethe mobile robots themselves as well as other solid objects movingin the environment. Thus, fundamental to the motion planningproblem of multi-agents is the need to plan and control themotions of the agents that yield inter-agent and agent-obstaclecollision avoidances.

Numerous papers have discussed this problem,using methods such as discretization of the configurationtime-space using sequential space slicing [3],sheared cylindrical representations of moving obstacles andgenerating optimal tangential paths to the goals [4],decomposition of the problem into path planning and velocityplanning sub-problems [5], threaded petri nets[6], plan-merging [7], negotiations [8], hybrid systems [9], onlineartificial potential fields strategy [10],and a Lyapunov-based control scheme for various nonholonomicmulti-agents [11-13], to name a few.

In this paper, we explore the challenging but indispensable area of multi-agent research by improving upon and extending the results of [12-13] to multiple*n*-link nonholonomic mobile manipulators. Another novel aspect of this paper is the inclusion of multiple rods and ellipses as stationary obstacles within the operating workspace of the mobile manipulators, wherein the positions and orientations of these obstacles are randomized. To achieve target convergence and to generate collision avoidances maneuvers, we will design acceleration controls of the multiple robots within the framework of the control scheme adopted from [13]. The control scheme, classified as the Lyapunov-based control scheme, algorithmically combines the principles of the Direct Method of Lyapunov and the artificial potential field method. The central idea behind this scheme is to design an appropriate Lyapunov function which acts as an artificial potential field function or *total potentials*. Accordingly, the scheme warrants the attachment of an attractive field to the target and a repulsive field to each obstacle, with the direction of motion facilitated via notion of steepest descent [13]. In addition, weaddress stability issues of the system via the integrated Lyapunov Method.

The rest of the paper is organized as follows: in Section II, the dynamic model of the *n*-link nonholonomic mobile manipulator is defined; in Section III, we deploy the Lyapunov-based control scheme by designing attractive and repulsive potential field functions; in Section IV, the acceleration controllers are designed and the stability analysis of the mobile manipulators is carried out; in Section V, computer simulation of an interesting scenario is presented; and Section VI concludes the paper and outlines future work in the area.

II. Vehicle Model

Let A_i, $i \in \{1,2,..,N\}$, $N \in \mathbb{N}$, represent the i th$n$-link nonholonomic mobile manipulator(nMM), where $n \in \mathbb{N}$. A_i

S. Singh is with the School of Computing, Information and Mathematical Sciences, Faculty of Science, Technology and Environment, The University of the South Pacific, Suva, Fiji Islands (e-mail: shonal.singh@usp.ac.fj).

S. Singh, B. Sharma, J. Vanualailai and A. Prasad are with the University of the South Pacific.

consists of a nonholonomic rear wheel car-like mobile platform with a *n*-link planar arm mounted on the mid-front axle of the platform [12-13]. As an illustration, Fig. 1 provides the schematics of a 3-link mobile manipulator, or 3MM, in the inertial frame $\aleph$.

With reference to Fig. 1, at time $t \geq 0$, $(x_i(t), y_i(t))$ denotes the position of the end-effector, $\phi_i(t)$ corresponds to the platform's steering angle with respect to its longitudinal axis, while ℓ_0 and b_0 are, respectively, the length and the width of the platform. Furthermore, ℓ_k is the length of link k, $k \in \{1,2,\ldots,n\}$. The reader is referred to Table I for a description of the variables that will be used to depict the dynamic model of A_i. For simplicity, we let each mobile manipulator system to be of the same dimension.

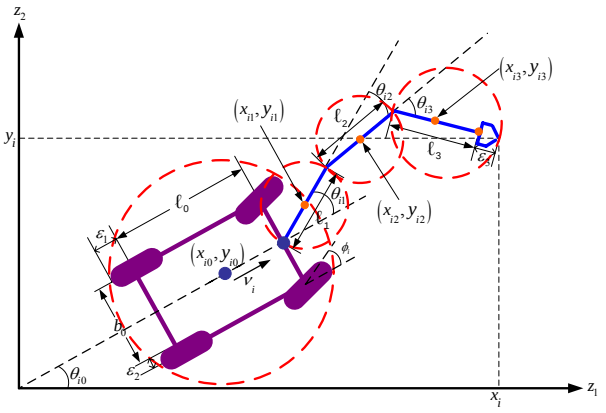

Fig. 1 Schematics of a 3MM in the inertial frame $\aleph$.

Adopting the nomenclature of [11-13], the dynamic model of A_i with respect to the position of the end-effector $(x_i, y_i) \in \mathbb{R}^2$, defined in the inertial frame $\aleph$, is derived as

$$\begin{aligned}
\dot{x}_i &= v_i \cos\theta_{i0} - \sum_{m=0}^{n}\left[\ell_m \sin\left(\sum_{p=0}^{m}\theta_{ip}\right)\right]\omega_{i0} \\
&\quad - \sum_{m=1}^{n}\left[\sum_{k=m}^{n}\ell_k \sin\left(\sum_{p=0}^{k}\theta_{ip}\right)\right]\omega_{im}, \\
\dot{y}_i &= v_i \sin\theta_{i0} + \sum_{m=0}^{n}\left[\ell_m \cos\left(\sum_{p=0}^{m}\theta_{ip}\right)\right]\omega_{i0} \\
&\quad + \sum_{m=1}^{n}\left[\sum_{k=m}^{n}\ell_k \cos\left(\sum_{p=0}^{k}\theta_{ip}\right)\right]\omega_{im}, \qquad (1) \\
\dot{\theta}_{im} &= \omega_{im}, \\
\dot{v}_i &= u_{i1}, \\
\dot{\omega}_{im} &= u_{i\,m+2},
\end{aligned}$$

where $m \in \{0,1,2,\ldots,n\}$. System (1) is a description of the instantaneous velocities and accelerations of the i th*n*MM. We shall use the vector notation $\mathbf{x}_i = (x_i, y_i, \theta_{i0}, \theta_{i1}, \theta_{i2}, \ldots, \theta_{in}, v_i, \omega_{i0}, \omega_{i1}, \omega_{i2}, \ldots, \omega_{in}) \in \mathbb{R}^{2n+5}$ to refer to the position and velocity components of A_i. For generality, we collect the states of all the N robots in the vector $\mathbf{x} = (\mathbf{x}_1, \mathbf{x}_2, \ldots, \mathbf{x}_N) \in \mathbb{R}^{(2n+5)\times N}$.

TABLE I
NOMENCLATURE OF A_i

Variable	Description
$x_{i0}(t)$	z_1 component of the position of the center of the platform
$y_{i0}(t)$	z_2 component of the position of the center of the platform
$x_{ik}(t)$	z_1 component of the position of the center of link k
$y_{ik}(t)$	z_2 component of the position of the center of link k
$\theta_{i0}(t)$	angular position of platform with respect to the z_1 axis
$\theta_{i1}(t)$	angular position of link 1 with respect to the platform
$\theta_{ik}(t)$	angular position of link k with respect to link $k-1$, $k = 2,3,\ldots,n$
$v_i(t)$	linear velocity of the wheels of the platform
$\omega_{i0}(t)$	angular velocity of the platform
$\omega_{ik}(t)$	angular velocity of link k
$u_{i1}(t)$	linear acceleration of the wheels of the platform
$u_{i2}(t)$	angular acceleration of the platform
$u_{i\,k+2}(t)$	angular acceleration of link k

Furthermore, we assume no slippage, that is,

$$\dot{x}_{ir}\sin\theta_{i0} - \dot{y}_{ir}\cos\theta_{i0} = 0,$$

and

$$\dot{x}_{if}\sin(\theta_{i0}+\phi_i) - \dot{y}_{if}\cos(\theta_{i0}+\phi_i) = 0,$$

and pure rolling, that is,

$$\dot{x}_{i0}\cos\theta_{i0} + \dot{y}_{i0}\sin\theta_{i0} = v_i,$$

where (x_{ir}, y_{ir}) and (x_{if}, y_{if}) are the Cartesian coordinates of the rear and front wheels of A_i, respectively. These generate non-integrable constraints of the wheeled platform, constraints that are denoted as the *nonholonomic constraints* of system (1)[13].

We can express the positions of the mobile platform and link k, where $k \in \{1,2,\ldots,n\}$, of A_i completely in terms of the state variables:

$$\left.\begin{aligned} x_{i0} &= x_i - \tfrac{\ell_0}{2}\cos\theta_{i0} - \sum_{k=1}^{n} \tfrac{\ell_k}{2^{\lfloor \frac{1}{k+1} \rfloor}} \cos\left(\sum_{p=0}^{k}\theta_{ip}\right), \\ y_{i0} &= y_i - \tfrac{\ell_0}{2}\sin\theta_{i0} - \sum_{k=1}^{n} \tfrac{\ell_k}{2^{\lfloor \frac{1}{k+1} \rfloor}} \sin\left(\sum_{p=0}^{k}\theta_{ip}\right), \end{aligned}\right\} \quad (2)$$

and

$$\left.\begin{aligned} x_{im} &= x_i - \sum_{k=m}^{n} \tfrac{\ell_k}{2^{\lfloor \frac{m+1}{k+1} \rfloor}} \cos\left(\sum_{p=0}^{k}\theta_{ip}\right), \\ y_{im} &= y_i - \sum_{k=m}^{n} \tfrac{\ell_k}{2^{\lfloor \frac{m+1}{k+1} \rfloor}} \sin\left(\sum_{p=0}^{k}\theta_{ip}\right), \end{aligned}\right\} \quad (3)$$

where equation (2) gives the Cartesian position (x_{i0}, y_{i0}) of the center of the platform and equation (3) gives the Cartesian position (x_{im}, y_{im}) of the center of the m thlink, $m = 1,2,\ldots,n$. These position constraints are known as the *holonomic constraints* of the mobile manipulator system[13].

To ensure that the entire body of A_i navigates around an obstacle safely, we enclose each articulated body of the robot by the smallest circle possible [11-13]. With reference to Fig. 1, given the *clearance parameters* ε_1 and ε_2, we can enclose the platform by a circular protective region centered at (x_{i0}, y_{i0}) with radius $r_0 = \frac{1}{2}\sqrt{(\ell_0 + 2\varepsilon_1)^2 + (b_0 + 2\varepsilon_2)^2}$. For link k, we use a circular protective region centered at (x_{ik}, y_{ik}) with radius $r_k = \frac{\ell_k}{2}$, where $k = 1,2,\ldots,n-1$. Moreover, for link n, we use a circular protective region centered at (x_{in}, y_{in}) with radius $r_n = \frac{\ell_n}{2} + \varepsilon_3$ (where ε_3 is the *safety parameter* needed to protect the gripper).

III. Deployment of the Control Scheme

The objective of this paper is to develop artificial potential fieldfunctions (APFs), and accordingly, design the translational and rotational accelerations, u_{i1} and $u_{i\,m+2}$, for $m = 0,1,2,\ldots,n$, respectively, within the framework of the Lyapunov-based control scheme, such that A_i will be able to carry out a number of subtasks before reaching its destination. The subtasks include: navigating in the obstacle-ridden environment; respecting the kinematic and dynamic constraints, and reaching the target position safely. The proposed APFs are distance functions formed in Euclidian space and the control scheme combines these APFs to form a Lyapunov function candidate – a platform to design the nonlinear controllers for A_i. This Lyapunov function candidate will also be utilized in a later section to prove stability of system (1).

Noting that for A_i, $i \in \{1,2,\ldots,N\}$, and $m \in \{0,1,2,\ldots,n\}$, for the m tharticulated body of A_i (or as stated otherwise), in the following subsections we will design the attractive functions for convergence and target attraction, and the repulsive functionsfor repelling the robot from specified obstacles.

A. Target Attraction

We affix a target for A_i to reach after some time $t > 0$. For the end-effector of A_i, the designated target is a disk with center (p_{i1}, p_{i2}) and radius $rt_i > 0$: $T_i = \left\{(z_1, z_2) \in \mathbb{R}^2 : (z_1 - p_{i1})^2 + (z_2 - p_{i2})^2 \le rt_i^2\right\}$.

For attraction to this target, we adopt the target attractive function

$$V_i(\mathbf{x}) = \frac{1}{2}\left[(x_i - p_{i1})^2 + (y_i - p_{i2})^2 + v_i^2 + \sum_{m=0}^{n}\omega_{im}^2\right].$$

B. Kinematic Constraints

The various types of obstacles populating the workspace and their necessary specifications are discussed below.

1) Workspace: Boundary Limitations

We consider a planar workspace, which is a fixed, closed, andbounded rectangular region defined for $\eta_1, \eta_2 > 2\sum_{m=0}^{n} r_m$, as $WS = \left\{(z_1, z_2) \in \mathbb{R}^2 : 0 \le z_1 \le \eta_1, 0 \le z_2 \le \eta_2\right\}$. The region's boundaries are defined as follows:

Left Boundary: $B_1 = \left\{(z_1, z_2) \in \mathbb{R}^2 : z_1 = 0\right\}$;

Lower Boundary: $B_2 = \left\{(z_1, z_2) \in \mathbb{R}^2 : z_2 = 0\right\}$;

Right Boundary: $B_3 = \left\{(z_1, z_2) \in \mathbb{R}^2 : z_1 = \eta_1\right\}$;

Upper Boundary: $B_4 = \left\{(z_1, z_2) \in \mathbb{R}^2 : z_2 = \eta_2\right\}$;

The boundaries have to be avoided by each articulated body of A_i at all time $t \ge 0$, so that the mobile manipulator is confined within the four boundaries of the workspace. For the avoidance by each articulated body of A_i, we design the following obstacle avoidance functions for the avoidance of the left, lower, right and upper boundaries, respectively:

$$\begin{aligned} W_{i\,4m+1}(\mathbf{x}) &= x_{im} - r_m, \\ W_{i\,4m+2}(\mathbf{x}) &= y_{im} - r_m, \\ W_{i\,4m+3}(\mathbf{x}) &= \eta_1 - (r_m + x_{im}), \\ W_{i\,4m+4}(\mathbf{x}) &= \eta_2 - (r_m + y_{im}). \end{aligned}$$

Here, $W_{i\,4m+1}(\mathbf{x}), W_{i\,4m+3}(\mathbf{x}) > 0$ for all $x_{im} \in (r_m, \eta_1 - r_m)$ and $W_{i\,4m+2}(\mathbf{x}), W_{i\,4m+4}(\mathbf{x}) > 0$ for all $y_{im} \in (r_m, \eta_2 - r_m)$, recalling that $\eta_1, \eta_2 > 2\sum_{m=0}^{n} r_m$.

To generate repulsive effects from the function W_{is}, $s = 1,2,\ldots,4n+4$, the Lyapunov-based control scheme warrants the design of a repulsive potential field function which is an inverse function that encodes the avoidance function to the denominator and a *tuning parameter* $\alpha_{is} > 0$ in the numerator[13]. This ratio inhibits the motion of the articulated robot to within the rectangular workspace.

Hereafter, all the obstacle avoidance functions will be appropriately coupled with tuning parameters to design the repulsive potential field functions to generate the obstacle avoidance maneuvers of A_i. The reader is referred to [13] for a detailed analysis of the effects of the obstacle avoidance functions and the resulting repulsive potential field functions.

2) Stationary Solid Objects

Category 1: Elliptical Obstacles

We fix $q \in \mathbb{N}$ stationary objects, within the boundaries of the WS. The l th obstacle is an ellipse in *nonstandard position* with center $\left(o_{l1}^{'}, o_{l2}^{'}\right)$. Precisely, the l th elliptical obstacle is *the nonstandard set* $E_l^{'} = \left\{ \left(z_1^{'}, z_2^{'}\right) \in \mathbb{R}^2 : \frac{\left(z_1^{'} - o_{l1}^{'}\right)^2}{\tilde{A}_l^2} + \frac{\left(z_2^{'} - o_{l2}^{'}\right)^2}{\tilde{B}_l^2} \le 1 \right\}$, where the $z_1^{'} z_2^{'}$ plane is measured with respect to the $z_1 z_2$ plane. The $z_1^{'} z_2^{'}$ plane is obtained by rotating the $z_1 z_2$ plane counterclockwise through the angle ψ_l. Also, the center $\left(o_{l1}^{'}, o_{l2}^{'}\right)$ is with respect to the $z_1^{'} z_2^{'}$ plane.

As shown in [12], the set $E_l^{'}$ can be rewritten with respect to the $z_1 z_2$ plane as

$$E_l = \left\{ \left(z_1, z_2\right) \in \mathbb{R}^2 : A_l^{'} + B_l^{'} \le 1 \right\},$$

where

$$A_l^{'} = \frac{\left[\left(z_1 - o_{l1}\right)\cos\psi_l + \left(z_2 - o_{l2}\right)\sin\psi_l \right]^2}{\tilde{A}_l^2},$$

$$B_l^{'} = \frac{\left[-\left(z_1 - o_{l1}\right)\sin\psi_l + \left(z_2 - o_{l2}\right)\cos\psi_l \right]^2}{\tilde{B}_l^2}.$$

We note that when $\psi_l = 0$, the l th elliptical obstacle is in *standard position* such that a *horizontal ellipse* is when $\tilde{A}_l > \tilde{B}_l$ and a *vertical ellipse* is when $\tilde{A}_l < \tilde{B}_l$. Moreover, if $\tilde{A}_l = \tilde{B}_l$ (for all values of ψ_l), the ellipse collapses into a circle with radius $\tilde{A}_l = \tilde{B}_l$.

For the avoidance of the l th obstacle by the m th articulated body of A_i, we consider the obstacle avoidance function

$$EO_{iml}\left(\mathbf{x}\right) = \frac{1}{2}\left[\hat{A}_{iml} + \hat{B}_{iml} - 1 \right],$$

where

$$\hat{A}_{iml} = \frac{\left[\left(x_{im} - o_{l1}\right)\cos\psi_l + \left(y_{im} - o_{l2}\right)\sin\psi_l \right]^2}{\left(\tilde{A}_l + r_m\right)^2},$$

$$\hat{B}_{iml} = \frac{\left[-\left(x_{im} - o_{l1}\right)\sin\psi_l + \left(y_{im} - o_{l2}\right)\cos\psi_l \right]^2}{\left(\hat{B}_l + r_m\right)^2},$$

for $l = 1, 2, \ldots, q$. The function $EO_{iml}\left(\mathbf{x}\right)$ is the measure of the Euclidian distance between the center of the l th obstacle and the m th articulated body of A_i.

Category 2: Rod-shaped Obstacles

We fix $z \in \mathbb{N}$ rod-shaped obstacles within the WS. Adopting the methodology of [13], we assume that the $\tilde{k}$ th rod-shaped obstacle is collapsed into a straight line segment with initial coordinates $\left(a_{\tilde{k}1}, b_{\tilde{k}1}\right)$ and final coordinates $\left(a_{\tilde{k}2}, b_{\tilde{k}2}\right)$. Thus, the $\tilde{k}$ th rod-shaped obstacle can be described by the set $S_{\tilde{k}} = \left\{ \left(z_1, z_2\right) \in \mathbb{R}^2 : \left(z_1 - c_{im\tilde{k}}\right) + \left(z_2 - d_{im\tilde{k}}\right) \right\}$, where $c_{im\tilde{k}} = a_{\tilde{k}1} + \lambda_{im\tilde{k}}\left(a_{\tilde{k}2} - a_{\tilde{k}1}\right)$ and $d_{im\tilde{k}} = b_{\tilde{k}1} + \lambda_{im\tilde{k}}\left(b_{\tilde{k}2} - b_{\tilde{k}1}\right)$ is its parametric representation, for $0 \le \lambda_{im\tilde{k}} \le 1$.

Adopting the minimum distance technique of [13] we identify the closest point of each $\tilde{k}$ th line segment measured from the reference point of the m th body of A_i. Avoidance of the closest point at any time $t \ge 0$ essentially results in the avoidance of the entire line segment by the complete A_i. Minimization of the Euclidian distance between the point $\left(x_{im}, y_{im}\right)$ and the $\tilde{k}$ th line segment $\left(c_{im\tilde{k}}, d_{im\tilde{k}}\right)$ yields

$$\lambda_{im\tilde{k}} = \left(x_{im} - a_{\tilde{k}1}\right) q_{\tilde{k}1} + \left(y_{im} - b_{\tilde{k}1}\right) q_{\tilde{k}2},$$

with

$$q_{\tilde{k}1} = \frac{a_{\tilde{k}2} - a_{\tilde{k}1}}{\left(a_{\tilde{k}2} - a_{\tilde{k}1}\right)^2 + \left(b_{\tilde{k}2} - b_{\tilde{k}1}\right)^2},$$

$$q_{\tilde{k}2} = \frac{b_{\tilde{k}2} - b_{\tilde{k}1}}{\left(a_{\tilde{k}2} - a_{\tilde{k}1}\right)^2 + \left(b_{\tilde{k}2} - b_{\tilde{k}1}\right)^2}.$$

In this research, we utilize the*saturation function* $\lambda_{im\tilde{k}} : \mathbb{R}^2 \to \left[0,1\right] \subset \mathbb{R}$ given as

$$\lambda_{im\tilde{k}}\left(c_{im\tilde{k}}, d_{im\tilde{k}}\right) = \begin{cases} 0 & , \text{ if } \lambda_{im\tilde{k}} < 0, \\ \lambda_{im\tilde{k}} & , \text{ if } 0 \le \lambda_{im\tilde{k}} \le 1, \\ 1 & , \text{ if } \lambda_{im\tilde{k}} > 1. \end{cases}$$

We note that $\lambda_{im\tilde{k}}\left(c_{im\tilde{k}}, d_{im\tilde{k}}\right)$ is a nonnegative scalar such that it is restricted to the interval $\left[0,1\right]$, implying that there is always an avoidance of the $\tilde{k}$ th rod-shaped obstacle at every iteration $t \ge 0$.

For the avoidance of the $\tilde{k}$ throd-shaped obstacle by the m th articulated body of A_i, we design the avoidance function

$$RO_{im\tilde{k}}\left(\mathbf{x}\right) = \frac{1}{2}\left[\left(x_{im} - c_{im\tilde{k}}\right)^2 + \left(y_{im} - d_{im\tilde{k}}\right)^2 - r_m^2 \right],$$

for $k = 1, 2, \ldots, z$. The function $RO_{im\tilde{k}}\left(\mathbf{x}\right)$ is the measure of the distance between the closest point of the $\tilde{k}$ throd-shaped obstacle and the center of the m th articulated bodyof A_i.

3) Moving Obstacles

Each solid body of the nMM is treated as moving obstacle for all the other nMMs in the WS. Thus, for the m th component of A_i to avoid the u th moving solid body of A_j, the avoidance function is

$$MO_{muij}\left(\mathbf{x}\right) = \frac{1}{2}\left[\left(x_i - x_j\right)^2 + \left(y_i - y_j\right)^2 - \left(r_m + r_u\right)^2 \right],$$

for $j = 1, 2, \ldots, N$, $j \neq i$.

C. Artificial Obstacles from Dynamic Constraints

The instantaneous velocities of the mobile platform and the n links of A_i are restricted due to safety considerations, and the rotation angles of link k, $k = 1, 2, \ldots, n$, are restricted due to mechanical singularities. These dynamic constraints can be treated within the Lyapunov-based control scheme by constructing *artificial obstacles* associated to each constraint and then avoiding them to yield the desired effect[11-13].

1) Modulus Bound on Velocities

We limit the translational and rotational velocities of A_i as follows:

(i) $|v_i| < v_{\max}$, where $v_{\max}$ is the *maximal achievable speed*;

(ii) $|\omega_{i0}| < \frac{v_{\max}}{|\rho_{\min}|}$, where $\rho_{\min} = \frac{\ell_0}{\tan(\phi_{\max})}$. This condition arises due to the boundness of the steering angle ϕ_i. That is, $|\phi_i| \leq \phi_{\max}$, where $\phi_{\max}$ is the *maximal steering angle*;

(iii) $|\omega_{im}| < \omega_{m\ \max}$, for $m = 1, 2, \ldots, n$, where $\omega_{m\ \max}$ is the *maximal rotational velocity* of link m of the n-link arm.

For simplicity, we assume that the values of $v_{\max}$, $\phi_{\max}$ and $\omega_{m\ \max}$, for $m = 1, 2, \ldots, n$, of every A_i are the same.

Now, based on the aforesaid constraints, we design an artificial obstacle tagged to each constraint [13]. For example, we construct the artificial obstacle $AO_{i1} = \{v_i \in \mathbb{R} : v_i \leq -v_{\max} \text{ or } v_i \geq v_{\max}\}$, to cater for the maximal achievable speed.

For the avoidance of these artificial obstacles, we design the following obstacle avoidance functions, respectively:

$$U_{i1}(\mathbf{x}) = \frac{1}{2}(v_{\max} - v_i)(v_{\max} + v_i),$$

$$U_{i2}(\mathbf{x}) = \frac{1}{2}\left(\frac{v_{\max}}{|\rho_{\min}|} - \omega_i\right)\left(\frac{v_{\max}}{|\rho_{\min}|} + \omega_i\right),$$

$$U_{i\ m+2}(\mathbf{x}) = \frac{1}{2}(\omega_{m\ \max} - \omega_{im})(\omega_{m\ \max} + \omega_{im}).$$

2) Mechanical Singularities

Singular configurations arisewhen $\theta_{im} = 0$, $\theta_{im} = \pi$ or $\theta_{im} = -\pi$, for $m = 2, 3, \ldots, n$. Accordingly, we impose the restriction $0 < |\theta_{im}| < \pi$, which means that the links of A_i can neither be fully stretched nor folded onto each other. The corresponding artificial obstacle is $AO_{i\ m+(n+1)} = \{\theta_{im} \in \mathbb{R} : \theta_{im} = 0,\ \theta_{im} = \pi \text{ or } \theta_{im} = -\pi\}$ and for avoidance, we construct the following functions:

$$S_{i\ 2m-3}(\mathbf{x}) = |\theta_{im}|, \qquad S_{i\ 2m-2}(\mathbf{x}) = \pi - |\theta_{im}|,$$

for $\theta_{im} \in (-\pi, 0) \cup (0, \pi)$ and $m = 2, 3, \ldots, n$.

We also note that the angle between link 1 and the mobile platform is bounded, that is, $\theta_{i1} \in (-\pi/2, \pi/2)$. To ensure that link 1 stays within this interval, we utilize

$$S_{i\ 2n-1}(\mathbf{x}) = \frac{1}{2}\left(\frac{\pi}{2} - \theta_{i1}\right)\left(\frac{\pi}{2} + \theta_{i1}\right),$$

for the avoidance of the artificial obstacle defined as $AO_{i\ 2n+2} = \{\theta_{i1} \in \mathbb{R} : \theta_{i1} \leq -\pi/2 \text{ or } \theta_{i1} \geq \pi/2\}$.

D. Auxiliary Function

To ensure that the potentials designed for A_i vanishes at its target configuration, we consider

$$F_i(\mathbf{x}) = \frac{1}{2}\left[(x_i - p_{i1})^2 + (y_i - p_{i2})^2\right],$$

as an appropriate auxiliary function.

IV. Controller Design and Stability Analysis

This section witnesses the extraction of the nonlinear control laws of system (1) via the Lyapunov-based control scheme. In parallel, we utilize Lyapunov's Direct Method to provide mathematical proof of stability of system (1).

A. Lyapunov Function

Combining all the attractive and repulsive potential functions and introducing *tuning parameters* (or *control parameters*), $\alpha_{is} > 0$, $\gamma_{iml} > 0$, $\sigma_{im\tilde{k}} > 0$, $\varphi_{muij} > 0$, $\xi_{ip} > 0$, and $\beta_{ir} > 0$, where $s, l, \tilde{k}, p, r \in \mathbb{N}$, $m, u = 0, 1, 2, \ldots, n$, and $j = 1, 2, \ldots, N$, $j \neq i$, we define a Lyapunov function candidate for system (1) as

$$L(\mathbf{x}) = \sum_{i=1}^{N}\left\{V_i(\mathbf{x}) + F_i(\mathbf{x})\left[\sum_{s=1}^{4n+4}\frac{\alpha_{is}}{W_{is}(\mathbf{x})} + \sum_{m=0}^{n}\sum_{l=1}^{q}\frac{\gamma_{iml}}{EO_{iml}(\mathbf{x})}\right]\right\}$$
$$+ \sum_{i=1}^{N}\left\{F_i(\mathbf{x})\sum_{m=0}^{n}\left[\sum_{\tilde{k}=1}^{z}\frac{\sigma_{im\tilde{k}}}{RO_{im\tilde{k}}(\mathbf{x})} + \sum_{\substack{j=1\\ j\neq i}}^{N}\sum_{u=0}^{n}\frac{\varphi_{muij}}{MO_{muij}(\mathbf{x})}\right]\right\}$$
$$+ \sum_{i=1}^{N}F_i(\mathbf{x})\left[\sum_{r=1}^{n+2}\frac{\beta_{ir}}{U_{ir}(\mathbf{x})} + \sum_{p=1}^{2n-1}\frac{\xi_{ip}}{S_{ip}(\mathbf{x})}\right].$$

B. Nonlinear Acceleration Controllers

For $i = 1, 2, \ldots, N$ and $m = 0, 1, 2, \ldots, n$, we have

$$f_{i1}=\left[1+\sum_{s=1}^{4n+4}\frac{\alpha_{is}}{W_{is}}+\sum_{m=0}^{n}\left(\sum_{l=1}^{q}\frac{\gamma_{iml}}{EO_{iml}}+\sum_{\tilde{k}=1}^{z}\frac{\sigma_{im\tilde{k}}}{RO_{im\tilde{k}}}+\sum_{\substack{j=1\\ j\neq i}}^{N}\sum_{u=0}^{n}\frac{\varphi_{muij}}{MO_{muij}}\right)+\sum_{p=1}^{2n-1}\frac{\xi_{ip}}{S_{ip}}+\sum_{r=1}^{n+2}\frac{\beta_{ir}}{U_{ir}}\right](x_i-p_{i1}),$$

$$f_{i2}=\left[1+\sum_{s=1}^{4n+4}\frac{\alpha_{is}}{W_{is}}+\sum_{m=0}^{n}\left(\sum_{l=1}^{q}\frac{\gamma_{iml}}{EO_{iml}}+\sum_{\tilde{k}=1}^{z}\frac{\sigma_{im\tilde{k}}}{RO_{im\tilde{k}}}+\sum_{\substack{j=1\\ j\neq i}}^{N}\sum_{u=0}^{n}\frac{\varphi_{muij}}{MO_{muij}}\right)+\sum_{p=1}^{2n-1}\frac{\xi_{ip}}{S_{ip}}+\sum_{r=1}^{n+2}\frac{\beta_{ir}}{U_{ir}}\right](y_i-p_{i2}),$$

$$g_{i1}=\frac{\xi_{i\ 2n-1}F_i}{S_{i\ 2n-1}^2}\theta_{i1},$$

$$g_{i\ n+1}=1+\frac{\beta_{i1}F_i}{U_{i1}^2},$$

$$g_{i\ n+(m+2)}=1+\frac{\beta_{i\ m+2}F_i}{U_{i\ m+2}^2},$$

$$\begin{aligned}f_{i\ 2m+3}=-F_i\Bigg\{&\frac{\alpha_{i\ 4m+1}}{W_{i\ 4m+1}^2}-\frac{\alpha_{i\ 4m+3}}{W_{i\ 4m+3}^2}\\&+\sum_{l=1}^{q}\frac{\gamma_{iml}}{EO_{iml}^2}\left[\frac{(x_{im}-o_{l1})\cos\psi_l+(y_{im}-o_{l2})\sin\psi_l}{\left(\tilde{A}_l+r_m\right)^2}\right]\cos\psi_l\\&-\sum_{l=1}^{q}\frac{\gamma_{iml}}{EO_{iml}^2}\left[\frac{(y_{im}-o_{l2})\cos\psi_l-(x_{im}-o_{l1})\sin\psi_l}{\left(\tilde{B}_l+r_m\right)^2}\right]\sin\psi_l\Bigg\}\\&-F_i\sum_{\tilde{k}=1}^{z}\frac{\sigma_{im\tilde{k}}}{RO_{im\tilde{k}}^2}\left\{(x_{im}-c_{im\tilde{k}})\left[1-(a_{\tilde{k}2}-a_{\tilde{k}1})q_{\tilde{k}1}\right]\right\}\\&+F_i\sum_{\tilde{k}=1}^{z}\frac{\sigma_{im\tilde{k}}}{RO_{im\tilde{k}}^2}\left\{(y_{im}-d_{im\tilde{k}})\left[1-(b_{\tilde{k}2}-b_{\tilde{k}1})q_{\tilde{k}1}\right]\right\}\\&+\sum_{\substack{j=1\\ j\neq i}}^{N}\sum_{u=0}^{n}\left[F_j\frac{\varphi_{umji}}{MO_{umji}^2}(x_{ju}-x_{im})-F_i\frac{\varphi_{muij}}{MO_{muij}^2}(x_{im}-x_{ju})\right],\end{aligned}$$

$$\begin{aligned}f_{i\ 2m+4}=-F_i\Bigg\{&\frac{\alpha_{i\ 4m+2}}{W_{i\ 4m+2}^2}-\frac{\alpha_{i\ 4m+4}}{W_{i\ 4m+4}^2}\\&+\sum_{l=1}^{q}\frac{\gamma_{iml}}{EO_{iml}^2}\left[\frac{(x_{im}-o_{l1})\cos\psi_l+(y_{im}-o_{l2})\sin\psi_l}{\left(\tilde{A}_l+r_m\right)^2}\right]\sin\psi_l\\&-\sum_{l=1}^{q}\frac{\gamma_{iml}}{EO_{iml}^2}\left[\frac{(y_{im}-o_{l2})\cos\psi_l-(x_{im}-o_{l1})\sin\psi_l}{\left(\tilde{B}_l+r_m\right)^2}\right]\cos\psi_l\Bigg\}\\&-F_i\sum_{\tilde{k}=1}^{z}\frac{\sigma_{im\tilde{k}}}{RO_{im\tilde{k}}^2}\left\{(y_{im}-d_{im\tilde{k}})\left[1-(b_{\tilde{k}2}-b_{\tilde{k}1})q_{\tilde{k}2}\right]\right\}\\&+F_i\sum_{\tilde{k}=1}^{z}\frac{\sigma_{im\tilde{k}}}{RO_{im\tilde{k}}^2}\left\{(x_{im}-c_{im\tilde{k}})\left[1-(a_{\tilde{k}2}-a_{\tilde{k}1})q_{\tilde{k}2}\right]\right\}\\&+\sum_{\substack{j=1\\ j\neq i}}^{N}\sum_{u=0}^{n}\left[F_j\frac{\varphi_{umji}}{MO_{umji}^2}(y_{ju}-y_{im})-F_i\frac{\varphi_{muij}}{MO_{muij}^2}(y_{im}-y_{ju})\right].\end{aligned}$$

Furthermore, for $i=1,2,\ldots,N$ and $m=2,3,\ldots,n$

$$g_{im}=-F_i\left(\frac{\xi_{i\ 2m-3}}{S_{i\ 2m-3}^2}-\frac{\xi_{i\ 2m-2}}{S_{i\ 2m-2}^2}\right)\frac{|\theta_{im}|}{\theta_{im}}.$$

Letting $g_{i0}=0$, $i=1,2,\ldots,N$, for $m=0,1,2,\ldots,n$ we can further define

$$\begin{aligned}G_{i1}&=\left(f_{i1}+\sum_{m=0}^{n}f_{i\ 2m+3}\right)\cos\theta_{i0}+\left(f_{i2}+\sum_{m=0}^{n}f_{i\ 2m+4}\right)\sin\theta_{i0},\\G_{i\ m+2}&=-\ell_m\left(f_{i1}+\frac{1}{2}f_{i\ 2m+3}\right)\sin\left(\sum_{p=0}^{m}\theta_{ip}\right)\\&\quad+\ell_m\left(f_{i2}+\frac{1}{2}f_{i\ 2m+4}\right)\cos\left(\sum_{p=0}^{m}\theta_{ip}\right)\\&\quad-\ell_m\sum_{k=m+1}^{n}f_{i\ 2k+3}\sin\left(\sum_{p=0}^{m}\theta_{ip}\right)\\&\quad+\ell_m\sum_{k=m+1}^{n}f_{i\ 2k+4}\cos\left(\sum_{p=0}^{m}\theta_{ip}\right)+g_{im}.\end{aligned}$$

Now, consider the following theorem:

Theorem 1: Consider multiple*n*-link nonholonomic mobile manipulators whose motionsare governed by ODEs described in system (1). The objective is to, amongst other integrated subtasks, control the motions of the robots within an obstacle-ridden environment. The subtasks include: restrictions placed on the workspace, convergence to predefined targets, and consideration of kinodynamic constraints. Utilizing the potential field functions the following continuous acceleration controllers can be generated for A_i, $i\in\{1,2,\ldots,N\}$:

$$\left.\begin{aligned}u_{i1}&=-(\delta_{i1}v_i+G_{i1})/g_{i\ n+1},\\u_{i\ m+2}&=-(\delta_{i\ m+2}\omega_{im}+G_{i\ m+2})/g_{i\ n+(m+2)},\end{aligned}\right\}$$

where $m\in\{0,1,2,\ldots,n\}$ and $\delta_{ih}>0$, for $h=1,2,\ldots,n+2$, are constants commonly known as *convergence parameters*.

Theorem 2: If the fixed point $\mathbf{x}_i^*=\left(p_{i1},p_{i2},\theta_{i0}^f,\theta_{i1}^f,\theta_{i2}^f,\ldots,\theta_{in}^f,0,0,0,0,\ldots,0\right)\in\mathbb{R}^{2n+5}$ is an equilibrium point of A_i, then $\mathbf{x}^*=\left(\mathbf{x}_1^*,\mathbf{x}_2^*,\ldots,\mathbf{x}_N^*\right)\in D\left(L(\mathbf{x})\right)$ is an equilibrium state of system (1). Here, θ_{im}^f, for $m\in\{0,1,2,\ldots,n\}$, denotes the final orientation of the mth articulated body of A_i at the center of its prescribed target.

Proof: For $i\in\{1,2,\ldots,N\}$ and $m\in\{0,1,2,\ldots,n\}$:

1) $L(\mathbf{x})$ is defined, continuous and positive over the domain
$D\left(L(\mathbf{x})\right)=\{W_{is}(\mathbf{x})>0;EO_{iml}(\mathbf{x})>0;RO_{im\tilde{k}}(\mathbf{x})>0;$

$MO_{muij}(\mathbf{x}) > 0; S_{ip}(\mathbf{x}) > 0; U_{ir}(\mathbf{x}) > 0\}$;

2) $L(\mathbf{x}^*) = 0$;

3) $\dot{L}(\mathbf{x}) > 0 \ \forall \mathbf{x} \in D(L(\mathbf{x}))/\mathbf{x}^*$.

The time derivative of L along every solution of system (1) is the dot product of the gradient of L, given by $\nabla L = \left(\frac{\partial L}{\partial \mathbf{x}_1}, \frac{\partial L}{\partial \mathbf{x}_2}, \ldots, \frac{\partial L}{\partial \mathbf{x}_N}\right)$, and the time-derivative of the state vector $\mathbf{x} = (\mathbf{x}_1, \mathbf{x}_2, \ldots, \mathbf{x}_N)$. This dot product is given as

$$\dot{L}(\mathbf{x}) = \sum_{i=1}^{N}\Bigg[f_{i1}\dot{x}_{i1} + f_{i2}\dot{y}_{i1} + \sum_{m=1}^{n} g_{im}\dot{\theta}_{im} + \sum_{m=0}^{n}\left(f_{i\,2m+3}\dot{x}_{im} + f_{i\,2m+4}\dot{y}_{im}\right) + g_{i\,n+1}v_i\dot{v}_i + \sum_{m=0}^{n} g_{i\,n+(m+2)}\omega_{im}\dot{\omega}_{im}\Bigg],$$

and substituting the controllers given in Theorem 1 and the governing ODEs for system (1) we secure a semi-negative definite function

$$\dot{L}(\mathbf{x}) = -\sum_{i=1}^{N}\left(\delta_{i1}v_i^2 + \sum_{m=0}^{n}\delta_{i\,m+2}\omega_{im}^2\right) \le 0.$$

Thus, $\dot{L}(\mathbf{x}) \le 0 \ \forall \mathbf{x} \in D(L(\mathbf{x}))$ and $\dot{L}(\mathbf{x}^*) = 0$. Finally, it can be easily verified that the first partials of $L(\mathbf{x})$ is C^1. Thus, $L(\mathbf{x})$ is a feasible Lyapunov function for system (1), and $\mathbf{x}^*$ isa stable equilibrium point in the sense of Lyapunov, provided the acceleration controllers are as defined in Theorem 1.

□

V. Simulation Results

This section considers the simulation results for four 3-link mobile manipulators (that is, $N = 4$ and $n = 3$) navigating in a constrained workspace cluttered with fixed obstacles. We verify numerically the stability results obtained from the Lyapunov function.

The workspace contains $q = 7$ elliptical obstacles, each with random positions and sizes. The parameter γ_{iml} has been randomized between 0 and 1, where $i = 1,2,3,4$, $m = 0,1,2,3$ and $l = 1,2,\ldots,7$. Additionally, the workspace is cluttered with $z = 7$ rod-shaped obstacles, each with random initial and final coordinates. The associated parameter $\sigma_{imk\tilde{}}$ has been randomized between 0 and 1, where $i = 1,2,3,4$, $m = 0,1,2,3$ and $\tilde{k} = 1,2,\ldots,7$. Note that for $i = 1,2,3,4$, the corresponding initial and final states of the 3MMs, workspace restrictions, numerical values of the different parameters and other essentials required to simulate the scenario are listed in Tables II and III.

Fig. 2 shows the paths taken by the 3MMs and their convergence to the desired goals. Enroute their desired goals, the mobile manipulators successfully evade collisions with the multiple moving and fixed obstacles intersecting their paths with the deployment of the acceleration controllers and appropriate values of the control parameters.

Fig. 3 and Fig. 5 show the behavior of the linear and angular velocities of the platforms of A_1 and A_2, respectively. Clearly, the translational velocities of the platforms of the two 3MMs decrease as they approach a moving/fixed obstacle and gain speed upon successful collision avoidance. Finally, the 3MMs slow down on approach to the target and eventually, at the center of the target the linear and angular velocities vanish. The behavior of the rotational velocities of the 3 links of the two manipulators are shown in Fig. 4 and Fig. 6, respectively, which also tend to zero as the robots approach their designated targets. With reference to Fig. 7, the orientation of each articulated body of A_4 stabilizes as the 3MM approaches its target. Similar trends were exhibited by the remaining 3MMs.

Fig. 8 and Fig. 9 show the time evolution of the relevant nonlinear controllers of A_1. One can notice the convergence of these controllers at the final configuration implying the effectiveness of the acceleration controllers. The corresponding graphs of the remaining 3MMs exhibited similar convergent properties along the system trajectories.

TABLE II
NUMERICAL VALUES OF INITIAL AND FINAL STATES

	Initial Configuration
Rectangular position	A_1: $(x_1(0), y_1(0)) = (8,5)$;
	A_2: $(x_2(0), y_2(0)) = (8,45)$;
	A_3: $(x_3(0), y_3(0)) = (42,45)$;
	A_4: $(x_4(0), y_4(0)) = (42,5)$
Angular positions	A_1: $\theta_{10}(0) = 0$, $\theta_{11}(0) = \pi/3$,
	$\theta_{12}(0) = -\pi/4$, $\theta_{13}(0) = -\pi/4$;
	A_2: $\theta_{20}(0) = 0$, $\theta_{21}(0) = \pi/3$,
	$\theta_{22}(0) = -\pi/4$, $\theta_{23}(0) = -\pi/4$;
	A_3: $\theta_{30}(0) = \pi$, $\theta_{31}(0) = -\pi/3$,
	$\theta_{32}(0) = \pi/4$, $\theta_{33}(0) = \pi/4$;
	A_4: $\theta_{40}(0) = \pi$, $\theta_{41}(0) = -\pi/3$,
	$\theta_{42}(0) = \pi/4$, $\theta_{43}(0) = \pi/4$;
Translational velocity	A_i: $v_i(0) = 1$
Rotational velocities	A_i: $\omega_{im}(0) = 0.05$, $m = 0,\ldots,3$
	Final Configuration
Target	A_1: $(p_{11}, p_{12}) = (49,45)$ and
	$rt_1 = 0.5$;
	A_2: $(p_{21}, p_{22}) = (49,5)$ and
	$rt_2 = 0.5$;
	A_3: $(p_{31}, p_{32}) = (1,5)$ and
	$rt_3 = 0.5$;
	A_4: $(p_{41}, p_{42}) = (1,45)$ and
	$rt_4 = 0.5$;

VI. Conclusion

This paper presents a generalized set of continuous, time-invariant acceleration control laws, derived from the Lyapunov-based control scheme, to guide multiple *n*-link nonholonomic mobile manipulators to their respective goals in a constrained workspace. In addition, this approach guaranteed the stability of the system in the sense of Lyapunov. The efficiency of the control laws was verified through computer simulations of four 3MMs operating within a virtual environment.

Future work includes extending the proposed technique to doubly nonholonomic mobile manipulators and modifying the proposed control algorithm for motion planning and control of mobile manipulators fixed in formation.

TABLE III
NUMERICAL VALUES OF CONSTRAINTS AND PARAMETERS

Constraints	
Dimension of A_i	$\ell_0 = 1.8$, $b_0 = 0.8$, and $\ell_1 = \ell_2 = \ell_3 = 0.8$
Max. velocities	$v_{\max} = 5$, $\omega_{1\max} = 1$, $\omega_{2\max} = 1$, $\omega_{3\max} = 1$
Max. steering angle	$\phi_{\max} = 7\pi/18$
Clearance parameters	$\varepsilon_1 = \varepsilon_2 = 0.1$, $\varepsilon_3 = 0.2$
WS boundaries	$\eta_1 = 50$, $\eta_2 = 50$
Elliptical obstacles	$(o_{l1}, o_{l2}) \in \{[5, \eta_1 - 5], [5, \eta_2 - 5]\}$, $(\tilde{A}_l, \tilde{B}_l) \in \{[0,4],[0,4]\}$, $\psi_l \in [-\pi, \pi]$, for $l = 1,\ldots,7$
Rod obstacles	$a_{\tilde{k}1} \in [5, \eta_1 - 5]$, $b_{\tilde{k}1} \in [5, \eta_2 - 5]$, $a_{\tilde{k}2} \in [a_{\tilde{k}1} - 5, a_{\tilde{k}1} + 5]$, $b_{\tilde{k}2} \in [b_{\tilde{k}1} - 5, b_{\tilde{k}1} + 5]$, for $\tilde{k} = 1,\ldots,7$
Parameters	
Boundary limitations	$\alpha_{is} = 0.01$, for $s = 1,\ldots,16$
Obstacle avoidance	$\gamma_{iml} \in [0,1]$, for $l = 1,\ldots,7$ and $\sigma_{im\tilde{k}} \in [0,1]$, for $\tilde{k} = 1,\ldots,7$, where $m = 0,\ldots,3$
Inter-robot avoidance	$\varphi_{muij} = 0.1$, for $j = 1,\ldots,4$, $j \neq i$ and $m,u = 0,\ldots,3$
Dynamic constraints	$\xi_{ip} = 0.005$, $\beta_{ir} = 0.005$, for $m,u = 0,\ldots,3$
Convergence	$\delta_{ih} = 500$, for $h = 1,\ldots,5$

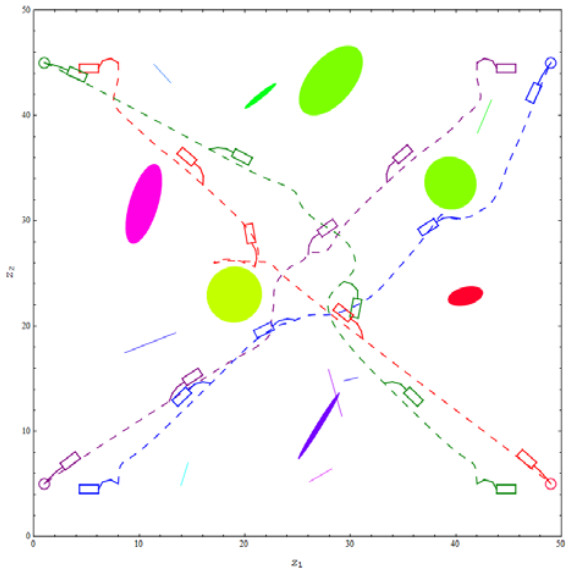

Fig. 2 Trajectory of the four 3MMs within a constrained environment

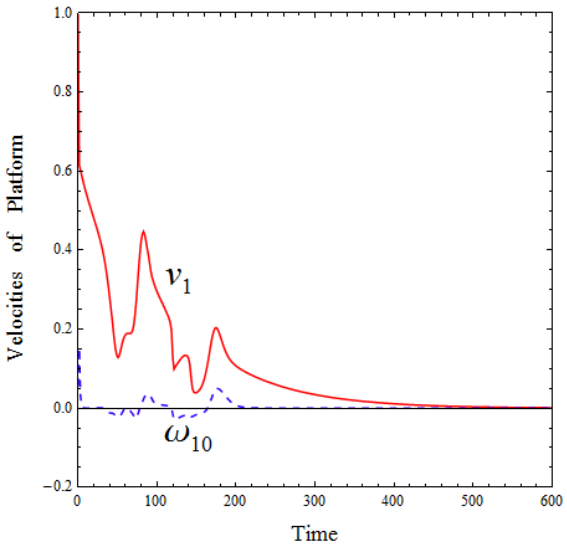

Fig. 3 Velocities of the wheeled platform of A_1.

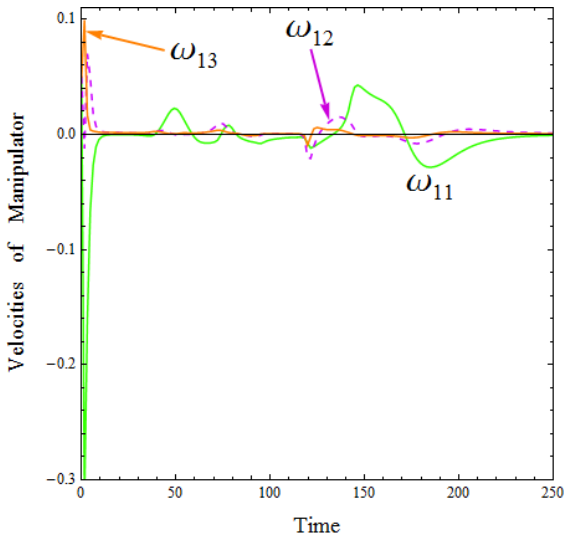

Fig. 4 Rotational velocities of the three links of A_1.

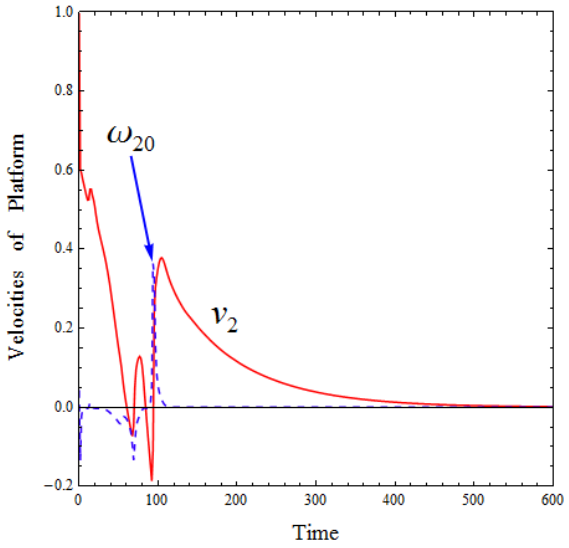

Fig. 5 Velocities of the wheeled platform of A_2.

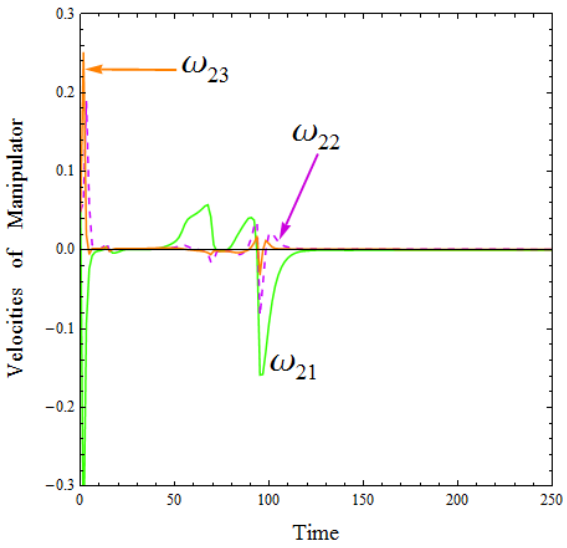

Fig. 6 Rotational velocities of the three links of A_2.

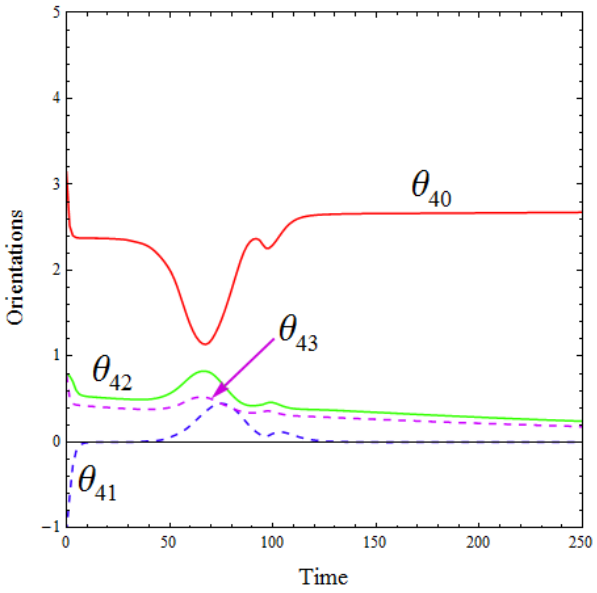

Fig. 7 Orientations of the various articulated bodies of A_4.

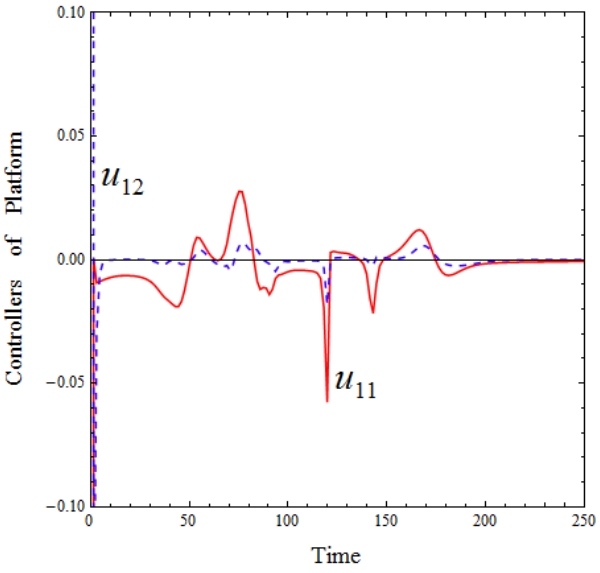

Fig. 8 Controllers of the wheeled platform of A_1.

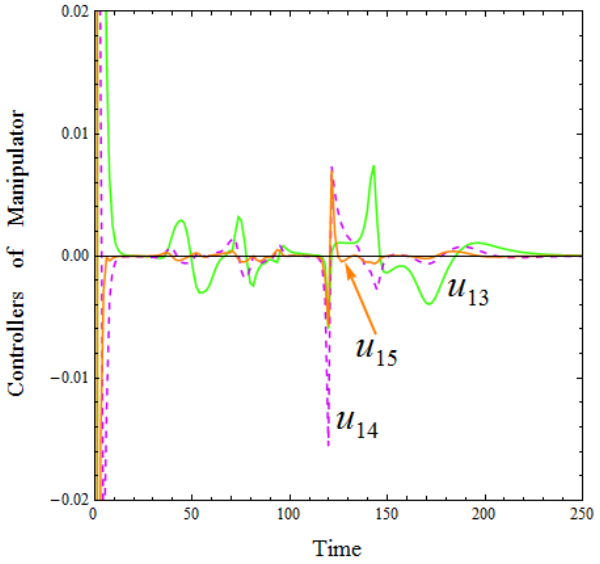

Fig. 9 Controllers of the three links of A_1

REFERENCES

[1] B. Sharma, J. Vanualailai, and A. Prasad. New Collision Avoidance Scheme for Multi-agents: A Solution to the Blindman's Problem. *Advances in Differential Equations and Control Processes*, 3(2):141–169, 2009.

[2] F. Arrichiello. *Coordination Control of Multiple Mobile Robots*. PhD dissertation, Universita Degli Studi Di Cassino, Cassino, Italy, November 2006. PhD Dissertation.

[3] M. Erdmann and T. Lozano-Perez. On Multiple Moving Objects. In *Proceedings of the IEEE International Conference on Robotics and Automation*, pp. 1419–1424, 1986.

[4] L. E. Parker. *A Robot Navigation Algorithm for Moving Obstacles*. Master's thesis, The University of Tennessee, Knoxville, 1988.

[5] K. Kant and S. W. Zucker. Toward Efficiency Trajectory Planning: The Path-velocity Decomposition. The International Journal of Robotics Research, 5(3):72–89, 1986.

[6] E. Klavins and D. E. Koditschek. Formalism for the Composition of Concurrent Robot Behaviors. In *Proceedings of the IEEE International Conference on Robotics and Automation*, pp. 3395–3402, San Francisco, CA, 2000.

[7] R. Alami, S. Fleury, M. Herrb, F. Ingrand, and F. Robert. Multi-robot Cooperation in the Martha Project. *IEEE Robotics & Automation Magazine*, 5:36–47, 1998.

[8] B. P. Gerkey and M. J. Mataric. Auction Methods for Multi-robot Coordination. In *IEEE Transactions on Robotics and Automation*, volume 8, pp. 758–768, 2002.

[9] M. Egerstedt and C. F. Martin. Conflict Resolution for Autonomous Vehicles: A Case Study in Hierarchical Control Design. *International Journal of Hybrid Systems*, 2(3):221-–234, 2002.

[10] D. Kostic, S. Adinandra, J. Caarls, and H. Nijmeijer. Collision-free Motion Coordination of Unicycle Multi-agent Systems. In 2010 American Control Conference, America, 2010.

[11] B. Sharma, J. Vanualailai, and S. Singh. Lyapunov-based Nonlinear Controllers for Obstacle Avoidance with a Planar *n*-link Doubly Nonholonomic Manipulator. *Robotics and Autonomous Systems*, 2012. http://dx.doi.org/10.1016/j.bbr.2011.03.031.

[12] S. Singh, B. Sharma, and J. Vanualailai. Autonomous Control of a Mobile Manipulator, *World Academy of Science, Engineering and Technology*, Issue 60, pp. 983–992, 2011.

[13] B. Sharma. *New Directions in the Applications of the Lyapunov-based Control Scheme to the Findpath Problem*. PhD dissertation, The University of the South Pacific, Fiji, 2008.